THE JOURNAL OF PHYSICAL CHEMISTRY B

Article

pubs.acs.org/JPCB

Localized Frustration and Binding-Induced Conformational Change in Recognition of 5S RNA by TFIIIA Zinc Finger

Cheng Tan, Wenfei Li,* and Wei Wang*

National Laboratory of Solid State Microstructure and Department of Physics, Nanjing University, Nanjing, Jiangsu 210093, China

Supporting Information

ABSTRACT: Protein TFIIIA is composed of nine tandemly arranged Cys_2His_2 zinc fingers. It can bind either to the 5S RNA gene as a transcription factor or to the 5S RNA transcript as a chaperone. Although structural and biochemical data provided valuable information on the recognition between the TFIIIIA and the 5S DNA/RNA, the involved conformational motions and energetic factors contributing to the binding affinity and specificity remain unclear. In this work, we conducted MD simulations and MM/GBSA calculations to investigate the binding-induced conformational changes in the recognition of the 5S RNA by the central three zinc fingers of TFIIIA and the energetic factors that influence the binding affinity and specificity at an atomistic level. Our results revealed drastic interdomain conformational changes between these three zinc fingers, involving the exposure/burial of several crucial DNA/RNA binding residues, which can be related to the competition between DNA and RNA for the binding of TFIIIA. We also showed that the specific recognition between finger 4/finger 6 and the 5S RNA introduces frustrations to the nonspecific interactions between finger 5 and the 5S RNA, which may be important to achieve optimal binding affinity and specificity.

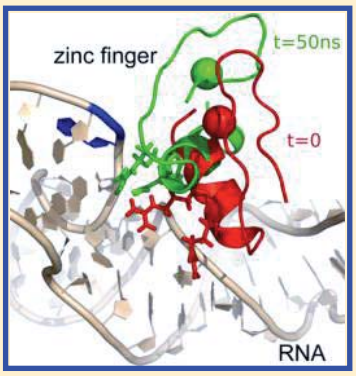

INTRODUCTION

Recognition of nucleic acids by proteins is fundamental to many biological processes. It was found that a number of proteins can bind both DNA and RNA, and play different functions in cell environment.[1−6] Such a bifunctional feature of proteins introduces an important issue about the mechanism by which the same protein binds to two kinds of nucleic acids that have quite distinct structures. TFIIIA, which consists of a tandem arrangement of nine classical Cys_2His_2 zinc fingers, is one of such proteins. Although named for its role as a transcription factor to regulate the expression of the 5S RNA genes by binding to the internal promoter,[7] protein TFIIIA was also shown to form a complex with the 5S RNA in a 7S ribonucleoprotein storage particle, acting as a 5S RNA chaperone.[8−10] Previously, it was found that both the 5S gene promoter and the 5S RNA show comparably high affinities for TFIIIA ($K_d \cong 1$ nM[11,12]), suggesting a potential autoregulation pathway of the 5S RNA synthesis.[7,13−15] Apparently, to understand the underlying molecular mechanism of such competitive recognition, it is important to characterize the physical factors contributing to the affinity and specificity for the binding of TFIIIA to the nucleic acids.

The recognition of DNA by TFIIIA has been relatively well understood. Biochemical experiments showed that its fingers 1−3, 5, and 7−9 bind into the major groove of the 5S RNA gene promoter,[16] whereas its fingers 4 and 6 act as spacers, spanning across the minor groove of DNA.[16,17] Such a binding fashion was further supported by structural data.[18−20] Particularly, in these structures, a canonical binding mode for specific protein−DNA recognition was revealed: hydrogen bonds between one strand of the DNA and the residues at positions −1, +3, and +6 of the α-helix of the finger contribute to the primary interactions, and hydrogen bonds between the other strand of the DNA and the side chain of the residue at position 2 of the α-helix contribute to the secondary interaction.[18−21]

In comparison, the molecular mechanism of the recognition of RNA by TFIIIA is far from clear. Biochemical data suggested that the minimal 5S RNA binding part consists of fingers 4−6 (zf456).[22,23] Structural data of the zf456−RNA complex revealed two modes of molecular recognition: finger 5 (zf5) interacts with the phosphate backbone of helix V, whereas finger 4 (zf4) and finger 6 (zf6) specifically bind to some individual bases in the "loop" regions[24] (Figure 1). However, there are no obvious canonical atomic interaction modes between the 5S RNA and TFIIIA as that observed in the TFIIIA−DNA recognition, and some important questions remain unanswered: (i) how do the conformations of the component fingers of the zf456 change in response to the binding of the 5S RNA? (ii) how does the binding of these three fingers interplay to achieve the balance between the affinity of specific and nonspecific RNA binding?

In this work, we try to gain some insights into the above questions by performing all-atom molecular dynamics (MD) simulations and molecular mechanics/generalized Born surface area[25] (MM/GBSA) calculations. Our results show that the binding of the 5S RNA induces the closing of the interface between fingers zf4 and zf5 and the opening of the interface

Received: May 27, 2013
Revised: November 21, 2013
Published: November 22, 2013

dx.doi.org/10.1021/jp4052165 | J. Phys. Chem. B 2013, 117, 15917−15925

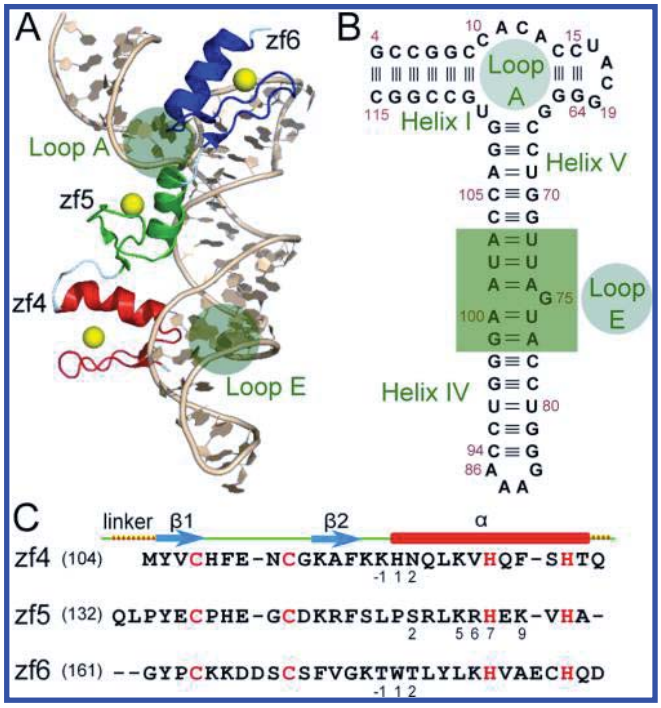

Figure 1. Crystal structure and sequence of the zf456−61mer 5S RNA complex. (A) Crystal structure of the zf456−5S RNA complex (PDB code: 1UN6). The three fingers are shown in different colors (zf4 in red, zf5 in green, and zf6 in blue), and the linker regions are shown in pale cyan. The yellow spheres represent the Zn^{2+} ions. (B) Sequence and the secondary structures of the 61mer 5S RNA. (C) Sequence and the corresponding secondary structures of zf456. The conserved Zn^{2+} binding residues "CCHH" are shown in red.

between fingers zf5 and zf6. We also observed frustration of the zf5−RNA interactions due to the restraint of the binding of zf4 and zf6 to RNA, which is important for the specific recognition between the zf4/zf6 and RNA.

METHODS

We used the X-ray crystal structure of the zf456−61mer 5S RNA complex (PDB code 1UN6[24]) as the initial condition. All MD simulations were carried out using the AMBER11 package[26] with the AMBER03 force field,[25,27,28] which has achieved success in simulating protein−nucleic acid complexes.[20,29−35] Independent MD simulations were performed for the zf456−5S RNA complex, the free zf456, and the free 5S RNA, respectively. We also conducted control MD simulations for both the zf456−5S RNA complex and the free zf456 with different combinations of removal of any two zinc fingers. Table 1 lists the detailed information of the simulations for all the systems mentioned above, including sequences, total number of atoms, time length of the MD simulations, and number of independent MD simulations.

All the systems were solvated in TIP3P water boxes.[36] K^+ and Cl^- ions were added to neutralize the net charge of the system and to mimic the ion concentration of 150 mM. Zn^{2+} and Mg^{2+} ions were added according to their Cartesian coordinates in the PDB file. In describing the interactions between the Zn^{2+} and protein, we did not consider the effects of charge transfer and protonation/deprotonation, since the current simulations do not involve the binding/unbinding of Zn^{2+} ions.[37] Instead, we used the "cationic dummy atom" (CaDA) model to reproduce the tetrahedral coordination of the zinc ion,[38] which has been successfully used in modeling the zinc finger−nucleic acid interactions.[35]

Table 1. Systems for MD Simulations

system	protein sequence	total number of atoms	MD length (ns)
free RNA		66071	7 × 50 = 350
free zf4	Y105−H129	10700	4 × 50 = 200
free zf5	Y135−H159	9430	4 × 50 = 200
free zf6	Y162−H188	10516	6 × 50 = 300
free zf456	M104−D190	48349	6 × 50 = 300
zf4 + RNA	Y105−H129	61537	4 × 50 = 200
zf5 + RNA	Y135−H159	66069	4 × 50 = 200
zf6 + RNA	Y162−H188	75030	4 × 50 = 200
zf456 + RNA	M104−D190	63800	6 × 50 = 300

In all the simulations, the non-bonded cutoff for long-range interactions was set to 12 Å, and the long-range electrostatic interactions were calculated using the particle mesh Ewald method.[39] The covalent bonds involving hydrogen atoms were constrained with the SHAKE algorithm,[40] and a time step of 0.002 ps was used. Before performing MD simulations, steepest descent and conjugated gradient energy minimization were carried out for each system. After minimization, the systems were heated to 300 K with harmonic restraints of 10 kcal/Å^2·mol on the solute atoms in the NVT ensemble and then equilibrated for 1 ns MD under the NPT conditions at 300 K and 1 atm pressure, with no restraints.

To look into the residue level details of the interaction between protein and RNA, we employed the pairwise energy decomposition scheme implemented in the MM/GBSA module[25] of the AMBER11 package.[26] In the energy decomposition, the solvent is treated implicitly using the generalized Born (GB) model[41] with the salt concentration set at 0.15 M. The hydrophobic interactions were described by the solvent accessible surface area (SASA) dependent term. By performing the energy decomposition, the energetic contributions of each finger to the TFIIIA−5S RNA interactions can be estimated. We note that the interactions between 5S RNA and zinc fingers include the contributions from the non-bonded terms, including the vdW term, the electrostatic term, and the solvation term, and therefore can be large values. However, in this work, the differences of these interaction terms between the real system and control system are more relevant to the conclusion of this work. In discussing the entropy contribution to the binding processes, we used the normal-mode analysis[42] implemented in the MM/GBSA module of the AMBER package.[26]

RESULTS AND DISCUSSION

Binding Induced Conformational Change of zf456. We used MD simulations with explicit water solvent to test whether the crystal structure of the zf456−5S RNA complex[24] is maintained in solution conditions. Figure 2 shows the RMSD values of the whole complex (black), the 5S RNA (green), and the zf456 (red) as functions of the simulation time for a representative trajectory, respectively. One can see that the zf456−5S RNA complex remains stable in solution environment as indicated by small RMSD values throughout the entire simulation. We conducted five independent MD simulations with different sets of initial velocities, and similar results were observed from all simulations.

dx.doi.org/10.1021/jp4052165 | J. Phys. Chem. B 2013, 117, 15917−15925

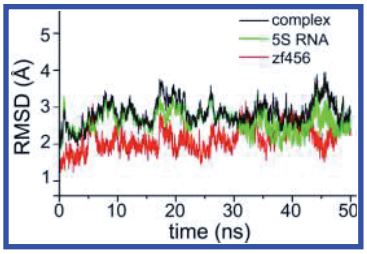

Figure 2. RMSD versus time for the zf456, the 5S RNA, and the whole complex with respect to the crystal structures.

We also performed MD simulations for the free zf456, starting from its crystal structure in complex. By comparing the conformations of the free zf456 obtained from simulations and those in the crystal structure of the zf456–RNA complex, we can identify the differences between these conformations of the zf456 with and without the binding of the 5S RNA. Figure 3A shows the RMSD values for the free zf456 and each of its three fingers, respectively. One can see that the RMSD of each finger maintains small values (~3 Å) during the simulations, indicating intradomain stability of these zinc fingers. In comparison, one can find that the whole zf456 undergoes obvious conformational change from the crystal structure (RMSD ~ 8 Å). Therefore, the preferred conformations for the free zf456 are largely different from that in the zf456–RNA complex; namely, the binding of the 5S RNA induces conformational change of the zf456. Apparently, such conformational change arises from the reorientation of the fingers. Similar conformational changes can also be observed in other independent MD simulations including a long simulation with a length of 300 ns (Figure S1, Supporting Information).

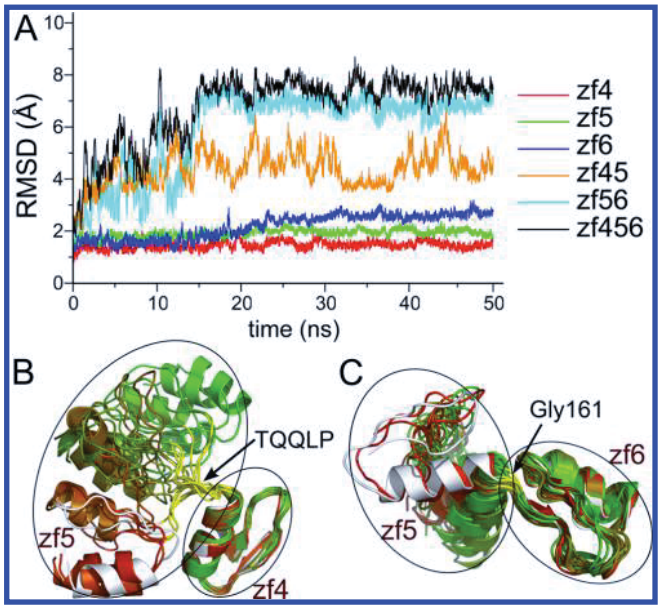

Figure 3. Conformational changes of free zf456 during the MD simulation. (A) RMSD versus simulation time for zf456 and its component parts including zf4, zf5, zf6, zf45, and zf56, respectively. (B) Superimposed zf45 structures of 20 snapshots evenly taken from one MD trajectory for the free zf456. In the superimposing, the conformations of zf4 were best fitted to its crystal structure. Two circles are used to separate the superimposing of zf4 and zf5. The crystal structure is colored in white, and colors of other snapshots gradually change from red to green, according to their simulation time. The "TQQLP" linker is shown in yellow color. (C) Same as part B but for the zf56 part.

To illustrate the interdomain motions between the fingers zf4 and zf5, we evenly picked up 20 snapshots from one representative MD trajectory of the free zf456 and superimposed these snapshots by fitting the conformation of zf4 to that in the crystal structure. With the zf4 fitted, the superimposing of these 20 conformations of zf5 is quite diverse (see Figure 3B). As the simulation proceeds, the spatial relationship between zf4 and zf5 quickly deviates from that of the crystal structure, resulting in more extended conformations of zf45. Such conformational change suggests that the binding of the 5S RNA induces the closing of the interface between zf4 and zf5. Similar interdomain motions were also observed between zf5 and zf6. Different from the zf45 part, however, the conformations of the zf56 part in the free zf456 are more compact than that in the crystal structure of the zf456–5S RNA complex (Figure 3C). Therefore, the binding with the 5S RNA requires the "opening" of the zf56 to expose certain specific protein–RNA interaction surface.

By employing the clustering analysis with the average linkage algorithm,[43] we assigned 3000 conformations of the zf45 sampled from six independent MD trajectories of the free zf456 into 50 clusters using RMSD as the distance metric. The largest value of the average distance to centroid of these 50 clusters is 1.05 Å, which guarantees the similarity of structures within each cluster. The cluster including the conformation of zf45 in the crystal structure is labeled as s_0, and the largest cluster which includes 771 conformations is labeled as s_1. Their representative structures are shown in Figure 4A and B, respectively, and the differences between these two structures are illustrated by the contact map in Figure 4C. The most obvious difference is that the side chain of residue Leu148, which forms a hydrophobic core with the side chains of residues Val124, Phe127, and Leu133 in the TFIIIA–5S RNA complex, detaches from the hydrophobic core and points outward to solvent in the free zf456 (Figure 4A, B, and C). This difference can be more clearly demonstrated by a negative correlation between the SASA of residue Leu148 and the number of interdomain contacts between zf4 and zf5 ($C_{4,5}$), as shown in Figure 4D. It is worth noting that residue Leu148 locates at the −1 position of the zf5 α-helix which makes canonical contacts with bases of the DNA in the TFIIIA–DNA complex, and is the only canonical DNA recognition residue which does not make contacts with the 5S RNA in the zf456–5S RNA complex. As indicated by our results, in the free zf456, the side chain of residue Leu148 tends to be exposed to solvent, and therefore is ready for the binding of the DNA. Whereas once zf456 is bound to the 5S RNA, the related DNA binding site is shielded by forming some interdomain hydrophobic contacts. As a result, this feature may lead to the reduction of the probability of substituted binding of the DNA. Such 5S RNA binding-induced conformational change of the DNA binding site tends to make the competition between the 5S RNA and the 5S DNA more cooperative, which is consistent with the autoregulation mechanism in the synthesis pathway of the 5S RNA.[1]

Similar to zf45, we carried out clustering analysis on the conformations for zf56 in the free zf456. We compared the representative structure of the largest cluster (s_1) with that of the crystal structure (Figure 5A, B, and C). Consistent with the results shown in Figure 3C, we observed that in the free zf456 the zf5 and zf6 domains established more contacts than those in the complex. Interestingly, these additional contacts involve the

dx.doi.org/10.1021/jp4052165 | J. Phys. Chem. B 2013, 117, 15917–15925

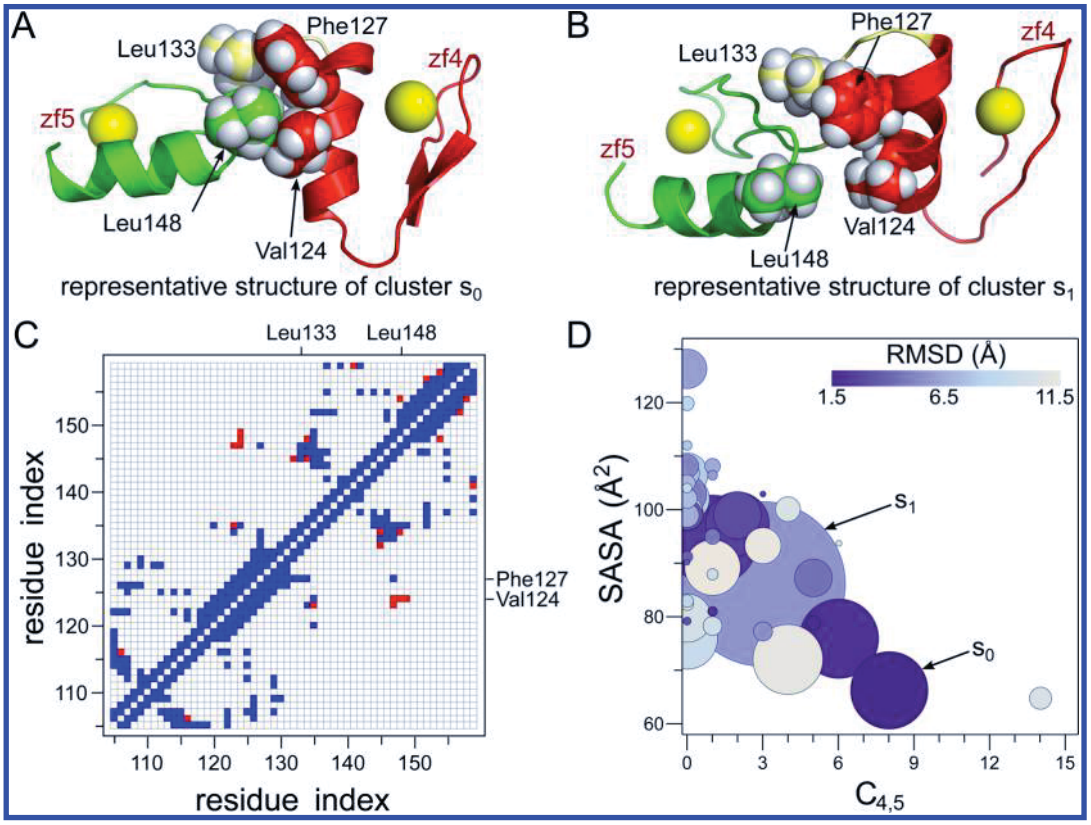

Figure 4. Features of the conformational change of zf45 using the clustering analysis. (A) The zf45 part of zf456 in the crystal structure, which is chosen as the representative structure of cluster s_0 of zf45. Side chains of residues Val124, Phe127, Leu133, and Leu148 are shown as spheres. Their heavy atoms in zf4 are shown in red, zf5 in green, and loop region in pale yellow. Zn^{2+} ions are shown as yellow spheres. (B) Representative structure of cluster s_1 for the zf45 part of zf456, which has the largest cluster size. Drawing methods and colors are the same as in part A. (C) Contact map of zf45 based on the representative structures of clusters s_0 and s_1. Blue dots represent the contacts that exist in both s_0 and s_1, and red dots represent the contacts appearing only in s_0. (D) Correlation plot of the number of contacts between zf4 and zf5 ($C_{4,5}$) and SASA of residue Leu148. Filled circles are used to represent the clusters, and their areas indicate the cluster sizes. Each circle is colored by the RMSD value of the representative structure of its corresponding cluster. The RMSD values are calculated with respect to the related crystal structure.

packing of the side chains from three residues, i.e., Arg154, Tyr162, and Trp177, which were found to interact with either bases or backbone groups of the 5S RNA in the zf456−5S RNA complex. In particular, the aromatic side chain of residue Trp177 forms a face-to-face stacking with the base of nucleic acid A11 in the complex, and therefore contributes to specific recognition[24,44] (see Figure 5A). To better illustrate the RNA binding-induced conformational change related with residue Trp177, we calculated the SASA of the side chain of Trp177 as a function of the number of interdomain contacts between zf5 and zf6 ($C_{5,6}$) (Figure 5D). It can be seen that in the largest cluster (s_1) of the zf56 part of free zf456, the zf5 and zf6 domains form more contacts with $C_{5,6}$ = 13 than those in the crystal structure (s_0) with $C_{5,6}$ = 8. Additionally, residue Trp177 is less exposed in the free zf456 with SASA ≃ 50 Å^2 than that in the crystal structure with SASA ≃ 105 Å^2. These results reveal that, in free zf56, the surface of the side chain of Trp177 is "blocked" by the side chain of residue Arg154 which interacts with the phosphate backbone of the 5S RNA in the protein−RNA complex (Figure 5A and B). On the basis of these results, we may conclude that the binding of the 5S RNA requires the opening of the zf5−zf6 interface to expose the key residues for establishing both specific and nonspecific contacts between the zf456 and 5S RNA.

Binding Induced Conformational Change of 5S RNA. We also studied the stability of the 5S RNA without the binding of TFIIIA based on the MD simulations of the free 61mer 5S RNA. We randomly selected 40 000 structures from five MD trajectories of the free RNA, and calculated the RMSD values of these structures with respect to the native crystal structure of the TFIIIA−5S RNA complex. The distribution of these RMSD values was shown in Figure 6A. As a comparison, a similar distribution of the RMSD values of RNA in the protein−RNA complex was also shown. It can be seen that, without the binding of the zinc fingers, i.e., the case of free RNA, the distribution shifts to larger values of RMSD. This behavior clearly suggests certain conformational changes of the 5S RNA due to the binding of zf456.

To find the conformational changes of the 5S RNA due to the binding of zf456, we calculated the RMSD for six parts of the 5S RNA, which are defined on the basis of their secondary structural characteristics. We observed that these parts are relatively stable both in the complex and in the free state, as indicated by their small values of RMSD (Figure S2, Supporting Information), which suggested that only minor changes of the secondary structural characteristics of the RNA helices took place upon the binding of zf456. However, by analyzing the distances and angles between these parts, we found that, upon the binding of zf456, the whole conformation of the 5S RNA is more compact, and the spatial relationship between these parts is changed (see Figure 6B). Parts C−E of Figure 6 additionally illustrate the details of these conformational differences. It can

dx.doi.org/10.1021/jp4052165 | J. Phys. Chem. B 2013, 117, 15917−15925

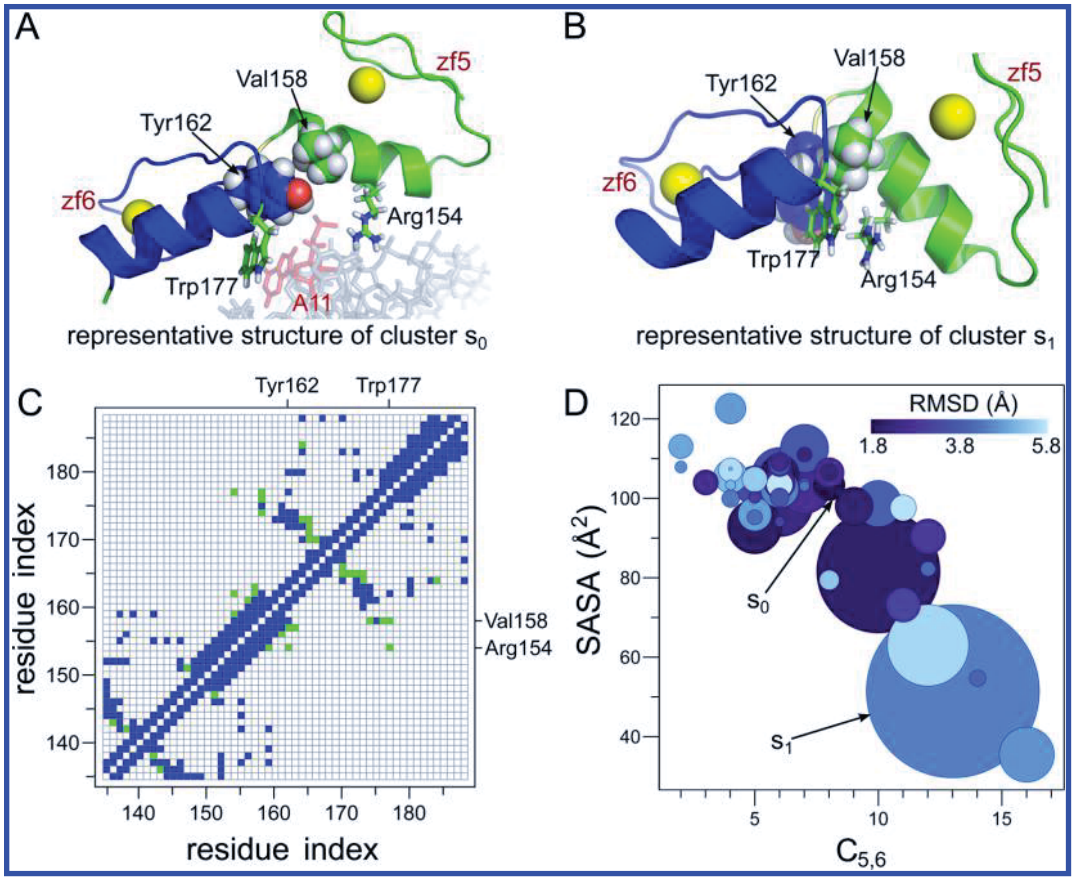

Figure 5. Features of the conformational change of zf56 using the clustering analysis. (A) The zf56 part of zf456 in the crystal structure, which is chosen as the representative structure of cluster s_0. The related part of RNA is added by referring to the crystal structure to show the stacking interaction between the base of A11 and the side chain of residue Trp177. Residues in zf5 are colored in green, zf6 in red, and the loop region in pale yellow. Zn^{2+} ions are shown as yellow spheres. (B) Representative structure of cluster s_1 for the zf56 part of zf456. (C) Contact map of zf56 based on the representative structures of s_0 and s_1. Blue dots represent the contacts that exist in both s_0 and s_1, and green dots represent the contacts that appear only in s_1. (D) Correlation plot of the number of contacts between zf5 and zf6 ($C_{5,6}$) and SASA of residue Trp177. Filled circles are used to represent the clusters, and their areas indicate the cluster sizes. Each circle is colored by the RMSD value of the representative structure of its corresponding cluster. The RMSD values are calculated with respect to the related crystal structure.

be seen in Figure 6C that, in the absence of zf456, most distances between the centroids of adjacent parts are larger than those in the zf456–RNA complex. Especially, large differences were observed for distances of helix I–helix IV and helix II–helix IV (Figure 6C), respectively. We found that the distance between helix I and helix IV decreases from ~49.6 to ~45.32 Å after being bound to zf456, whereas helix II is closer (~4 Å) to helix IV in the free RNA than in the zf456–RNA complex. In addition, we calculated the angles formed between the centroids of these parts, and found that the angle formed between helix I–loop A–helix IV (θ_1) in the complex is about 10° which is smaller than that in the free RNA, and θ_2 is ~10° larger in the complex (Figure 6D and E). Note that helix I and loop A are the zf5 and zf6 binding sites. Therefore, these results illustrate the zf456 binding-induced conformational changes of the 5S RNA, which involve a slight tightening of the whole structure and reorientation of several protein-binding related parts. Such binding-induced deformation of the 5S RNA may contribute to the binding affinity, as demonstrated in other protein–nucleic acids interactions.[45]

Localized Frustration in zf456–5S RNA Interactions. It is well-known that the delicate balance between affinity of the specific binding and nonspecific binding is crucial for successful protein–nucleic acid recognition.[46−48] To investigate the roles played by each single zinc finger in the TFIIIA–5S RNA recognition, we performed MD simulations for three control systems. In each of the control simulations, only one finger is included in the zf456–5S RNA complex. The initial structures for the simulations were prepared by removing the other two fingers from the crystal structure of the complex. We monitored the contacts formed between proteins and RNA, and found that the zf4–RNA and zf6–RNA complexes maintain most of the native contacts during the simulations (Figure S3, Supporting Information). However, the zf5–RNA interface changed drastically from the initial structure during the 50 ns simulations, as indicated by the Q-value of this interface, which is a measure of the nativeness (Figure S4, Supporting Information). We found that the Q-value of the zf5–RNA interface decreased rapidly in an early stage of the simulation, and at the end of the simulation, less than 40% of the native contacts were preserved (Figure S4, Supporting Information). Specifically, in all the repeated independent simulations for zf5–RNA, similar motions of rotation and sliding of zf5 on the RNA surface were observed. As an example, we compared two structures corresponding to the first and last snapshots of a representative 50 ns MD simulation trajectory, to illustrate the changes of the zf5–RNA interface. Figure 7 shows the contact map (Figure 7A) and superimposed structures (Figure 7B) of

dx.doi.org/10.1021/jp4052165 | J. Phys. Chem. B 2013, 117, 15917–15925

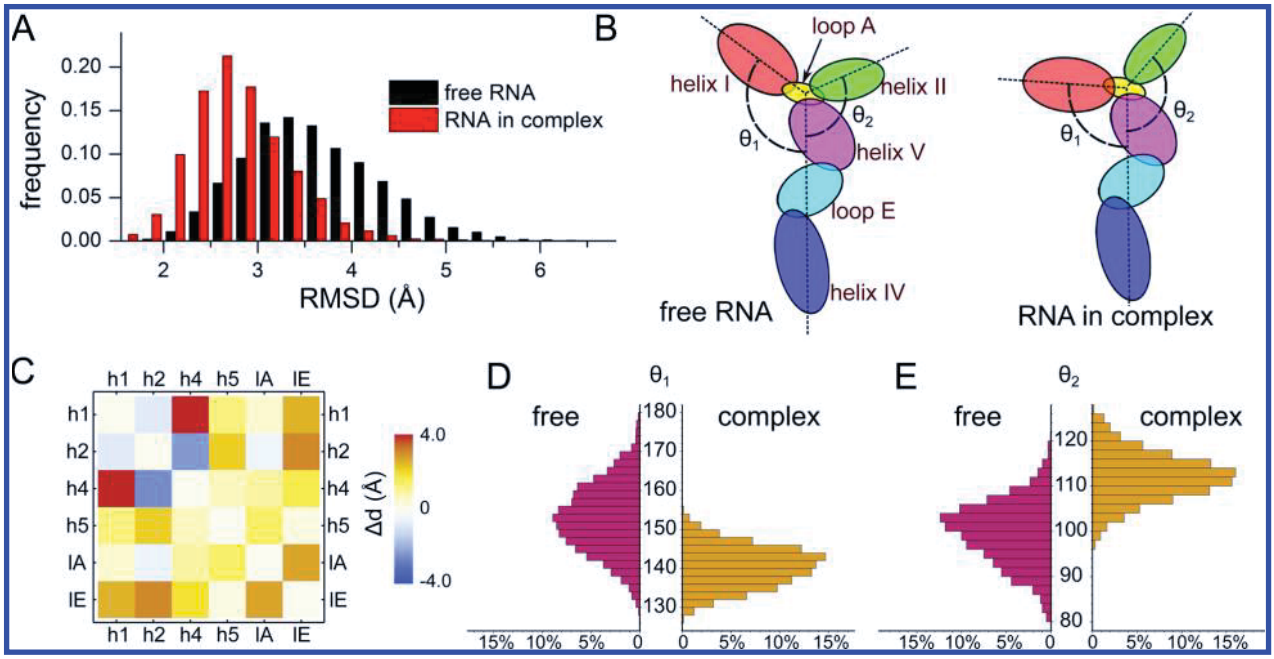

Figure 6. Conformational change of the 5S RNA in response to the binding of zf456. (A) Distribution of the RMSD values of the 5S RNA with respect to the crystal structure in the simulations of free RNA (black) and protein−RNA complex (red). These results are based on 40 000 conformations from five different MD simulations of the free RNA and 40 000 conformations from five simulations of the zf456−RNA complex. (B) Schematic representation of the six parts of the 5S RNA, which are defined on the basis of their secondary structure features. θ_1 is the angle defined by centroids of helix I−loop A−helix IV, and θ_2 is the angle of helix II−loop A−helix IV. (C) Change of the distances between the parts of RNA defined: $\Delta d = d_{free} - d_{complex}$, where d_{free} represents the average distances between the parts in the free 5S RNA and $d_{complex}$ represents those in the complex. (D and E) Distributions of angles defined in part B for free RNA and RNA in complex, respectively.

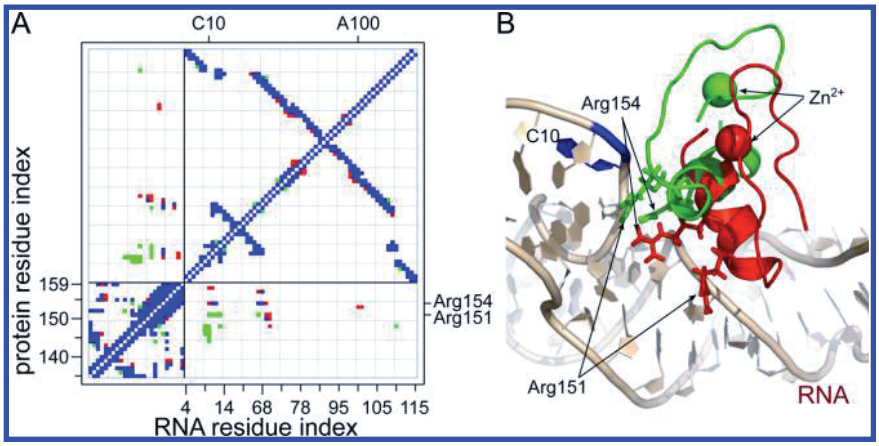

Figure 7. Changes of the zf5−RNA interface. (A) Contact map of the zf5−RNA complex for both the initial structure and the last structure of a representative 50 ns simulation trajectory of the zf5−RNA complex. Blue squares indicate contacts present in both structures. Red (or green) squares represent contacts present only in the initial structure (or the last structure), respectively. (B) The initial structure (in red) and the last structure (in green) of the zf5−RNA complex are superimposed by best fitting the RNA structure. Residues Arg151 and Arg154 are shown for both structures. Nucleic acid C10 in loop A of the RNA is shown in blue.

the zf5−RNA complex for the above two snapshots. We can see that most of the native zf5−RNA contacts are lost after 50 ns of simulation, except for several contacts formed around residue Arg154, suggesting that the zf5 rotates on the surface of the RNA using residue Arg154 as a pivot. Besides, the results revealed that residue Arg151 interacts with the helix V region of the 5S RNA in the initial structure and alters to form contact with nucleic acid C10 in loop A at the end of the simulation (Figure 7B). Such structural differences suggest that the contacts between the zf5 and RNA in the native complex do not correspond to the most stable binding mode.

The crystal structure of the zf456−RNA complex shows that the fingers zf4 and zf6 contribute most of the sequence specific recognition to the 5S RNA, whereas the zf5 binds nonspecifically to the backbone of the 5S RNA.[24,49−51] The conformational similarity between the one-finger−RNA systems and the full three-finger−RNA complex for the zf4/zf6−RNA binding demonstrates that the physical interactions determining the native structure of zf456−RNA also favor the one-finger zf4/zf6−RNA conformations, which implies that these conformations locate at the bottom of basins of the energy landscape. This is in accord with the "consistence principle" proposed in the protein folding field.[52] In comparison, for the finger zf5,

dx.doi.org/10.1021/jp4052165 | J. Phys. Chem. B 2013, 117, 15917−15925

Table 2. Interaction Energy Terms between the Zinc Fingers and the 5S RNA in the Control Simulations for zf4−5S RNA, zf5−5S RNA, and zf6−5S RNA (left) and in the Simulations for the zf456−5S RNA Complex (right), Respectively[a]

	control simulations			zf456−RNA complex			
	zf4−RNA	zf5−RNA	zf6−RNA	zf4−RNA	zf5−RNA	zf6−RNA	total
$E_{ele} + E_{GB}$	−42.6	−62.6	−24.3	−43.3	−56.5	−22.9	−124.9
E_{vdW}	−15.4	−13.3	−18.6	−17.5	−14.2	−21.1	−53.9
E_{SA}	−0.02	−0.02	−0.03	−0.02	−0.02	−0.02	−0.06

[a]These energies are calculated on the basis of summation of the decomposed pairwise energies between the protein residues and the RNA residues. The units of the energies are kcal/mol.

which contributes to nonspecific recognition, the most stable binding mode is distorted due to the restraint imposed by the specific binding of zf4 and zf6, suggesting the existence of frustration. This frustration illustrates that the zf4/6-restrained conformation for zf5 in the zf456−RNA complex locates at the margin of a certain basin of the energy landscape; therefore, in the absence of zf4/6, it has conformational changes even within a relatively short simulation time.

In addition to the MD simulations with explicit solvent, we also analyzed the interactions contributed by each finger, using the energy decomposition strategy implemented in the MM/GBSA module of the AMBER11 package[26] As can be seen in Table 2, the electrostatic term ($E_{ele} + E_{GB}$) of the intermolecule interaction between the finger zf5 and the 5S RNA is −62.6 kcal/mol. However, in the zf456−RNA complex, the electrostatic interactions between the zf5 and the 5S RNA are −56.5 kcal/mol, which is ∼6.1 kcal/mol weaker than that in the zf5−RNA complex. In comparison, the zf4 (zf6) in the zf456−RNA complex has quite similar values of electrostatic interaction energies as that in the zf4−RNA (zf6−RNA) complexes. For the vdW term (E_{vdW}) and surface area dependent term (E_{SA}), there are no obvious differences between the control systems and the full complex. These results suggest that the electrostatic interactions between the zf5 domain and the 5S RNA mostly favor the conformations observed in the zf5−RNA complex. Nevertheless, in the context of the whole zf456−RNA complex, to satisfy the specific contacts between the zf4 (zf6) and RNA, the zf5 tends to adopt a less stable binding mode, and therefore introduces certain frustration. The importance of localized frustrations imposed by the functional requirement was also observed in folding[53,54] and allosteric transitions[55−58] of proteins in the residual level. Here, we demonstrated that similar frustrations can also be observed in the protein−RNA recognition in the domain level, in order to achieve balance between the affinity of the specific and nonspecific binding.

Other than the intermolecule interaction energy, we also studied the entropy contributions of the zinc finger domains to the binding affinity employing the normal-mode analysis method[42] implemented in the MM/PBSA module of the AMBER11 software.[26] For the one-finger−RNA control complexes, namely, zf4−RNA, zf5−RNA, and zf6−RNA, the entropy contributions ($-T\Delta S$) are 40.3, 40.0, and 36.2 kcal/mol, respectively. Note that these values are comparable to those found in similar zinc finger−nucleic acid systems.[35] We found that the total binding entropy for zf456−RNA, $-T\Delta S$ = 88.5 kcal/mol, is less than the sum of the individual one-finger contributions. As the dominant entropic factors are from the low-frequency modes which represent large-scale collective motions among many domains,[59] we thus did not calculate the entropy contribution of each zinc finger domain in the zf456−RNA system, which cannot reflect the global motion of the multidomain zf456−RNA binding. The comparison of the total binding entropy in the real system and the control system suggests that the entropy contribution of multidomain protein complexes cannot be explained by a simple additive manner.

CONCLUSION

In this study, we used all-atom MD simulations with explicit solvent and MM/GBSA methodology to investigate the conformational changes of protein TFIIIA and the 5S RNA during the binding process, and the factors contributing to the binding affinity and specificity in the TFIIIA−5S RNA complex at an atomistic level. Our results demonstrated that the binding of the 5S RNA induces the closing of the interface between the fingers zf4 and zf5 and the opening of the interface between the fingers zf5 and zf6 of TFIIIA. We found that these RNA binding induced interdomain motions involve the exposure/burial of several crucial nucleic acid binding sites of TFIIIA, which may be involved in the competition between the 5S RNA and 5S DNA for the binding of TFIIIA. Similarly, we observed that due to the binding of TFIIIA conformational changes of the 5S RNA exist, which may contribute to the binding affinity.

In addition, the roles of each zinc finger domain were analyzed by combining the MM/GBSA analysis and energy decomposition. We showed that the specific recognition between the fingers zf4 (or zf6) and the 5S RNA introduces frustrations to the nonspecific interactions between the zf5 and the 5S RNA. These results provided insight into the molecular mechanism by which the fingers interplay to achieve balanced binding affinity for specific and nonspecific binding.

ASSOCIATED CONTENT

Supporting Information

Additional details describing the MD simulation time length, analysis of the simulation data, and miscellaneous derivations are provided in Figures S1−S4. This material is available free of charge via the Internet at http://pubs.acs.org.

AUTHOR INFORMATION

Corresponding Authors

*E-mail: wfli@nju.edu.cn (W.L.). Phone: +86 25 83686031. Fax: +86 25 83595535.

*E-mail: wangwei@nju.edu.cn (W.W.). Phone: +86 25 83686031. Fax: +86 25 83595535.

Notes

The authors declare no competing financial interest.

ACKNOWLEDGMENTS

The authors thank Shoji Takada and Naoto Hori for helpful discussions. This work was supported by the National Natural Science Foundation of China (No. 11174134, 81121062 and 91127026, 11111140012) and also by the 973 program (2013CB834104) and PAPD. Computational support from

Shanghai Supercomputer Center and HPCC of Nanjing University is acknowledged.

REFERENCES

(1) Cassiday, L. A.; Maher, L. J., III. Having It Both Ways: Transcription Factors That Bind DNA and RNA. *Nucleic Acids Res.* **2002**, *30*, 4118−4126.

(2) Zhai, G.; Iskandar, M.; Barilla, K.; Romaniuk, P. Characterization of RNA Aptamer Binding by the Wilms' Tumor Suppressor Protein WT1. *Biochemistry* **2001**, *40*, 2032−2040.

(3) Font, J.; Mackay, J. Beyond DNA: Zinc Finger Domains as RNA-Binding Modules. *Methods Mol. Biol. (Clifton, N.J.)* **2010**, *649*, 479−491.

(4) Graves, L.; Segal, S.; Goodwin, E. TRA-1 Regulates the Cellular Distribution of the Tra-2 mRNA in C. Elegans. *Nature* **1999**, *399*, 802−805.

(5) Dubnau, J.; Struhl, G. RNA Recognition and Translational Regulation by a Homeodomain Protein. *Nature* **1996**, *379*, 694−699.

(6) Ahn, J.; Prives, C. The C-Terminus of p53: The More You Learn the Less You Know. *Nat. Struct. Biol.* **2001**, *8*, 730−732.

(7) Pelham, H. R.; Brown, D. D. A Specific Transcription Factor That Can Bind Either the 5S RNA Gene or 5S RNA. *Proc. Natl. Acad. Sci. U.S.A.* **1980**, *77*, 4170−4174.

(8) Picard, B.; Wegnez, M. Isolation of a 7S Particle from Xenopus Laevis Oocytes: A 5S RNA-Protein Complex. *Proc. Natl. Acad. Sci. U.S.A.* **1979**, *76*, 241−245.

(9) Guddat, U.; Bakken, A.; Pieler, T. Protein-Mediated Nuclear Export of RNA: 5S rRNA Containing Small RNPs in Xenopus Oocytes. *Cell* **1990**, *60*, 619−628.

(10) Steitz, J.; Berg, C.; Hendrick, J.; La Branche-Chabot, H.; Metspalu, A.; Rinke, J.; Yario, T. A 5S rRNA/L5 Complex Is a Precursor to Ribosome Assembly in Mammalian Cells. *J. Cell Biol.* **1988**, *106*, 545−556.

(11) Sands, M. S.; Bogenhagen, D. F. The Carboxyterminal Zinc Fingers of TFIIIA Interact with the Tip of Helix V of 5S RNA in the 7S Ribonucleoprotein Particle. *Nucleic Acids Res.* **1991**, *19*, 1791−1796.

(12) You, Q.; Veldhoen, N.; Baudin, F.; Romaniuk, P. J. Mutations in 5S DNA and 5S RNA Have Different Effects on the Binding of Xenopus Transcription Factor IIIA. *Biochemistry* **1991**, *30*, 2495−2500.

(13) Barciszewska, M.; Szymaski, M.; Erdmann, V.; Barciszewski, J. Structure and Functions of 5S rRNA. *Acta Biochim. Pol.* **2001**, *48*, 191−198.

(14) Rollins, M.; Del Rio, S.; Galey, A.; Setzer, D.; Andrews, M. Role of TFIIIA Zinc Fingers in vivo: Analysis of Single-Finger Function in Developing Xenopus Embryos. *Mol. Cell. Biol.* **1993**, *13*, 4776−4783.

(15) Pittman, R.; Andrews, M.; Setzer, D. A Feedback Loop Coupling 5S rRNA Synthesis to Accumulation of a Ribosomal Protein. *J. Biol. Chem.* **1999**, *274*, 33198−33201.

(16) Clemens, K.; Liao, X.; Wolf, V.; Wright, P.; Gottesfeld, J. Definition of the Binding Sites of Individual Zinc Fingers in the Transcription Factor IIIA-5S RNA Gene Complex. *Proc. Natl. Acad. Sci. U.S.A.* **1992**, *89*, 10822−10826.

(17) Hayes, J.; Tullius, T. Structure of the TFIIIA-5S DNA Complex. *J. Mol. Biol.* **1992**, *227*, 407−417.

(18) Nolte, R. T.; Conlin, R. M.; Harrison, S. C.; Brown, R. S. Differing Roles for Zinc Fingers in DNA Recognition: Structure of a Six-Finger Transcription Factor IIIA Complex. *Proc. Natl. Acad. Sci. U.S.A.* **1998**, *95*, 2938−2943.

(19) Wuttke, D.; Foster, M.; Case, D.; Gottesfeld, J.; Wright, P. Solution Structure of the First Three Zinc Fingers of TFIIIA Bound to the Cognate DNA Sequence: Determinants of Affinity and Sequence Specificity. *J. Mol. Biol.* **1997**, *273*, 183−206.

(20) Tsui, V.; Radhakrishnan, I.; Wright, P. E.; Case, D. A. NMR and Molecular Dynamics Studies of the Hydration of a Zinc Finger-DNA Complex. *J. Mol. Biol.* **2000**, *302*, 1101−1117.

(21) Wolfe, S.; Nekludova, L.; Pabo, C. DNA Recognition by Cys2His2 Zinc Finger Proteins. *Annu. Rev. Biophys. Biomol. Struct.* **2000**, *29*, 183−212.

(22) Clemens, K.; Wolf, V.; McBryant, S.; Zhang, P.; Liao, X.; Wright, P.; Gottesfeld, J. Molecular Basis for Specific Recognition of Both RNA and DNA by a Zinc Finger Protein. *Science* **1993**, *260*, 530−533.

(23) Searles, M. A.; Lu, D.; Klug, A. The Role of the Central Zinc Fingers of Transcription Factor IIIA in Binding to 5S RNA. *J. Mol. Biol.* **2000**, *301*, 47−60.

(24) Lu, D.; Alexandra Searles, M.; Klug, A. Crystal Structure of a Zinc-Finger-RNA Complex Reveals Two Modes of Molecular Recognition. *Nature* **2003**, *426*, 96−100.

(25) Bashford, D.; Case, D. A. Generalized Born Models of Macromolecular Solvation Effects. *Annu. Rev. Phys. Chem.* **2000**, *51*, 129−152.

(26) Case, D. A.; Darden, T. A.; Cheatham, T. E.; Simmerling, C. L.; Wang, J.; Duke, R. E.; Luo, R.; Walker, R. C.; Zhang, W.; Merz, K. M., et al. *AMBER 11*; University of California: San Francisco, CA, 2008.

(27) Duan, Y.; Wu, C.; Chowdhury, S.; Lee, M.; Xiong, G.; Zhang, W.; Yang, R.; Cieplak, P.; Luo, R.; Lee, T. A Point-Charge Force Field for Molecular Mechanics Simulations of Proteins Based on Condensed-Phase Quantum Mechanical Calculations. *J. Comput. Chem.* **2003**, *24*, 1999−2012.

(28) Junmei, W.; Cieplak, P.; Kollman, P. A. How Well Does a Restrained Electrostatic Potential (RESP) Model Perform in Calculating Conformational Energies of Organic and Biological Molecules? *J. Comput. Chem.* **2000**, *21*, 1049−1074.

(29) Mackerell, A. D.; Nilsson, L. Molecular Dynamics Simulations of Nucleic Acid-Protein Complexes. *Curr. Opin. Struct. Biol.* **2008**, *18*, 194−199.

(30) Chen, Y. C.; Lim, C. Common Physical Basis of Macromolecule-Binding Sites in Proteins. *Nucleic Acids Res.* **2008**, *36*, 7078−7087.

(31) Da, L.-T.; Pardo Avila, F.; Wang, D.; Huang, X. A Two-State Model for the Dynamics of the Pyrophosphate Ion Release in Bacterial RNA Polymerase. *PLoS Comput. Biol.* **2013**, *9*, e1003020.

(32) Raju, R. K.; Burton, N. A.; Hillier, I. H. Modelling the Binding of HIV-Reverse Transcriptase and Nevirapine: An Assessment of Quantum Mechanical and Force Field Approaches and Predictions of the Effect of Mutations on Binding. *Phys. Chem. Chem. Phys.* **2010**, *12*, 7117−7125.

(33) Tsuda, K.; Kuwasako, K.; Takahashi, M.; Someya, T.; Inoue, M.; Terada, T.; Kobayashi, N.; Shirouzu, M.; Kigawa, T.; Tanaka, A.; Sugano, S.; Güntert, P.; Muto, Y.; Yokoyama, S. Structural Basis for the Sequence-Specific RNA-Recognition Mechanism of Human CUG-BP1 RRM3. *Nucleic Acids Res.* **2009**, *37*, 5151−5166.

(34) Wang, D.; Zhu, G.; Huang, X.; Lippard, S. J. X-Ray Structure and Mechanism of RNA Polymerase II Stalled at an Antineoplastic Monofunctional Platinum-DNA Adduct. *Proc. Natl. Acad. Sci. U.S.A.* **2010**, *107*, 9584−9589.

(35) Lee, J.; Kim, J.-S.; Seok, C. Cooperativity and Specificity of Cys_2His_2 Zinc Finger Protein-DNA Interactions: A Molecular Dynamics Simulation Study. *J. Phys. Chem. B* **2010**, *114*, 7662−7671.

(36) Jorgensen, W. L.; Chandrasekhar, J.; Madura, J. D.; Impey, R. W.; Klein, M. L. Comparison of Simple Potential Functions for Simulating Liquid Water. *J. Chem. Phys.* **1983**, *79*, 926−935.

(37) Li, W.; Zhang, J.; Wang, J.; Wang, W. Metal-Coupled Folding of Cys2His2 Zinc-Finger. *J. Am. Chem. Soc.* **2008**, *130*, 892−900.

(38) Pang, Y. Novel Zinc Protein Molecular Dynamics Simulations: Steps Toward Antiangiogenesis for Cancer Treatment. *J. Mol. Biol.* **1999**, *5*, 196−202.

(39) Darden, T.; Perera, L.; Li, L.; Pedersen, L. New Tricks for Modelers from the Crystallography Toolkit: The Particle Mesh Ewald Algorithm and Its Use in Nucleic Acid Simulations. *Structure* **1999**, *7*, R55−R60.

(40) Ryckaert, J.-P.; Ciccotti, G.; Berendsen, H. J. Numerical Integration of the Cartesian Equations of Motion of a System with

Constraints: Molecular Dynamics of N-Alkanes. *J. Comput. Phys.* **1977**, *23*, 327−341.
(41) Onufriev, A.; Bashford, D.; Case, D. A. Exploring Protein Native States and Large-Scale Conformational Changes with a Modified Generalized Born Model. *Proteins* **2004**, *55*, 383−394.
(42) Case, D. A. Normal Mode Analysis of Protein Dynamics. *Curr. Opin. Struct. Biol.* **1994**, *4*, 285−290.
(43) Shao, J.; Tanner, S. W.; Thompson, N.; Cheatham, T. E. Clustering Molecular Dynamics Trajectories: 1. Characterizing the Performance of Different Clustering Algorithms. *J. Chem. Theory Comput.* **2007**, *3*, 2312−2334.
(44) Lee, B. M.; Xu, J.; Clarkson, B. K.; Martinez-Yamout, M. A.; Dyson, H. J.; Case, D. A.; Gottesfeld, J. M.; Wright, P. E. Induced Fit and "Lock and Key" Recognition of 5S RNA by Zinc Fingers of Transcription Factor IIIA. *J. Mol. Biol.* **2006**, *357*, 275−291.
(45) Dyson, H. J. Roles of Intrinsic Disorder in Protein-Nucleic Acid Interactions. *Mol. BioSyst.* **2012**, *8*, 97−104.
(46) Vuzman, D.; Levy, Y. Intrinsically Disordered Regions as Affinity Tuners in Protein-DNA Interactions. *Mol. BioSyst.* **2012**, *8*, 47−57.
(47) Rohs, R.; Jin, X.; West, S. M.; Joshi, R.; Honig, B.; Mann, R. S. Origins of Specificity in Protein-DNA Recognition. *Annu. Rev. Biochem.* **2010**, *79*, 233−69.
(48) Lunde, B. M.; Moore, C.; Varani, G. RNA-Binding Proteins: Modular Design for Efficient Function. *Nat. Rev. Mol. Cell Biol.* **2007**, *8*, 479−490.
(49) Gupta, A.; Gribskov, M. The Role of RNA Sequence and Structure in RNA−Protein Interactions. *J. Mol. Biol.* **2011**, *409*, 574−587.
(50) Oberstrass, F. C.; Lee, A.; Stefl, R.; Janis, M.; Chanfreau, G.; Allain, F. H.-T. Shape-Specific Recognition in the Structure of the Vts1p SAM Domain with RNA. *Nat. Struct. Mol. Biol.* **2006**, *13*, 160−167.
(51) Stefl, R.; Skrisovska, L.; Allain, F. H.-T. RNA Sequence- and Shape-Dependent Recognition by Proteins in the Ribonucleoprotein Particle. *EMBO Rep.* **2005**, *6*, 33−38.
(52) Go, N. Theoretical Studies of Protein Folding. *Annu. Rev. Biophys. Biomol. Struct.* **1983**, *12*, 183−210.
(53) Sutto, L.; Lätzer, J.; Hegler, J. A.; Ferreiro, D. U.; Wolynes, P. G. Consequences of Localized Frustration for the Folding Mechanism of the IM7 Protein. *Proc. Natl. Acad. Sci. U.S.A.* **2007**, *104*, 19825−19830.
(54) Ferreiro, D. U.; Hegler, J. A.; Komives, E. A.; Wolynes, P. G. Localizing Frustration in Native Proteins and Protein Assemblies. *Proc. Natl. Acad. Sci. U.S.A.* **2007**, *104*, 19819−19824.
(55) Li, W.; Wolynes, P. G.; Takada, S. Frustration, Specific Sequence Dependence, and Nonlinearity in Large-Amplitude Fluctuations of Allosteric Proteins. *Proc. Natl. Acad. Sci. U.S.A.* **2011**, *108*, 3504−3509.
(56) Ferreiro, D. U.; Hegler, J. A.; Komives, E. A.; Wolynes, P. G. On the Role of Frustration in the Energy Landscapes of Allosteric Proteins. *Proc. Natl. Acad. Sci. U.S.A.* **2011**, *108*, 3499−3503.
(57) Levy, Y.; Cho, S. S.; Shen, T.; Onuchic, J. N.; Wolynes, P. G. Symmetry and Frustration in Protein Energy Landscapes: A Near Degeneracy Resolves the Rop Dimer-Folding Mystery. *Proc. Natl. Acad. Sci. U.S.A.* **2005**, *102*, 2373−2378.
(58) Marcovitz, A.; Levy, Y. Frustration in Protein-DNA Binding Influences Conformational Switching and Target Search Kinetics. *Proc. Natl. Acad. Sci. U.S.A.* **2011**, *108*, 17957−17962.
(59) Go, N.; Noguti, T.; Nishikawa, T. Dynamics of a Small Globular Protein in Terms of Low-Frequency Vibrational Modes. *Proc. Natl. Acad. Sci. U.S.A.* **1983**, *80*, 3696−3700.